

Formation of hierarchical LiMn_2O_4 dual-porous nanostructures by pyrolysis of gel precursor

Yanhua Tong, Yingying Li, Wanyu Lv, Zhenzhen Zhao, Min Zhang

Department of Chemistry, Huzhou Teachers College, Huzhou 313000, People's Republic of China
E-mail: tyh@hutc.zj.cn

Published in Micro & Nano Letters; Received on 25th February 2013; Accepted on 12th March 2013

A precursor-pyrolysing route to fabricate hierarchical LiMn_2O_4 porous nanostructures is presented. The product was characterised by X-ray powder diffraction, scanning electron microscopy, a transmission electron microscope, a high-resolution transmission electron microscope and a micromeritics analyser. The results show that the resulting material is a honeycomb-like dual-porous structure. One is quasi-hemispherical macropores of several hundred nanometres and the other is slit mesopores of several nanometres. This dual-porous nanostructure is composed of many ultrafine nanocrystallites whose size mainly falls into the range from 3 to 10 nm. Moreover, it has a large Brunauer–Emmett–Teller-specific surface area of $116\text{ m}^2/\text{g}$. The formation of such dual pores should be attributed to the Kirkendall effect and surface diffusion.

1. Introduction: Among numerous transition-metal oxides, manganese oxide-based compounds are particularly attractive as a lithium battery cathode because of their low cost, abundance and no toxicity [1, 2]. Spinel LiMn_2O_4 has emerged as one of the promising candidates owing to its three-dimensional Li^+ diffusion and high theoretical capacity of 148 mAh/g [3]. Nonetheless, the spinel LiMn_2O_4 suffers from capacity fading during cycling, which has been a key problem prohibiting LiMn_2O_4 from commercialisation.

The electrochemical properties of electrode materials strongly depend on physical and chemical properties such as particle size, morphology, stoichiometry and homogeneity [4, 5]. Nanomaterials with large surface area and small size as cathodes can shorten the Li-ion diffusion path and increase surface chemical activity, resulting in improvements in the performance of cathodes. Thus, various techniques were attempted to fabricate nanosized LiMn_2O_4 , including one-pot resorcinol-formaldehyde calcining [6], high-energy ball milling [7], ultrasonic waves [8], sol–gel [9, 10], the Pechini process [11], combustion [12] and the hydrothermal method [13]. These studies show that nanosized LiMn_2O_4 exhibit excellent rate capability, retaining its capacity at high rate; nanosized particles may have a stabilised surface that inhibits dissolution.

Here, hierarchical LiMn_2O_4 porous nanostructures were prepared via a precursor-pyrolysing route, employing lithium acetate and manganese acetate as Li–Mn source, citric acid as a chelating and combusting agent. The resulting product presents a three-dimensional honeycomb-like porous nanostructure, whose bulk structure is made up of nanocrystallites of about 10 nm. Its Brunauer–Emmett–Teller (BET)-specific surface area is $116\text{ m}^2/\text{g}$. It is larger than that of reported LiMn_2O_4 nanoparticles prepared by other methods. The influencing factors on the formation of hierarchical porous nanostructures were also investigated.

2. Experimental: All reagents were commercial compounds and of analytical purity grade. A typical procedure for preparation was similar to those described previously [14]: a 1:2 (mol) stoichiometric proportion of lithium acetate ($\text{Li}(\text{CH}_3\text{COO})_2 \cdot 2\text{H}_2\text{O}$) and manganese acetate ($\text{Mn}(\text{CH}_3\text{COO})_2 \cdot 4\text{H}_2\text{O}$) were dissolved in a minimum volume of ethanol. Then, an aqueous solution of citric acid (1.5 g) was dropwise added as a chelating and combusting agent into the above ethanol solution. The above mixture was magnetically stirred until a transparent solution was formed, then evaporated at

60°C for about 4 h to obtain transparent sol and was then dried at 120°C for about 6 h to yield gel precursors. The resultant gel precursor was annealed at 300°C for 0.5 h in air before cooling to room temperature naturally.

TG–DTA analysis of a gel precursor was carried out on an HCT-2 thermo analyser in air. The Fourier transform infrared (FTIR) spectra of the gel precursor and pure citric acid were measured by the KBr pellet method with a Nicolcol 5700 FTIR spectrometric analyser.

The phase and crystal graphic of the resultant products were characterised by X-ray diffraction (XRD) pattern, which was recorded by using a Shimadzu XRD-6000 X-ray diffractometer equipped with $\text{Cu K}\alpha$ radiation ($\lambda = 0.15406\text{ nm}$), the scanning rate of $0.05^\circ/\text{s}$ was applied to record the pattern in the 2θ range of $10\text{--}80^\circ$.

The morphology was characterised by a field emission scanning electron microscope (SEM, FEI Co., model Quanta-200, 15 kV). A microstructure study was conducted using a high-resolution transmission electron microscope (HRTEM) with an FEI Tecnai F20 transmission electron microscope (TEM), with an accelerating voltage of 200 kV. BET nitrogen adsorption–desorption was measured using a Micromeritics ASAP 2020 V3.01 H analyser.

3. Results and discussion

3.1. Composition and thermal analysis of the gel precursor: Figs. 1a and b show the FTIR spectra of pure citric acid and the gel precursor, respectively. In Fig. 1a, the broad absorption band

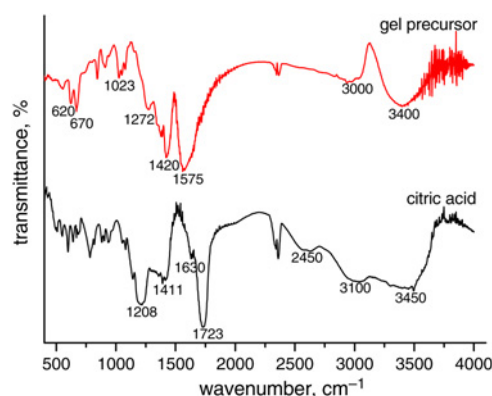


Figure 1 FTIR spectra of various samples: gel precursor (upper) and citric acid (lower)

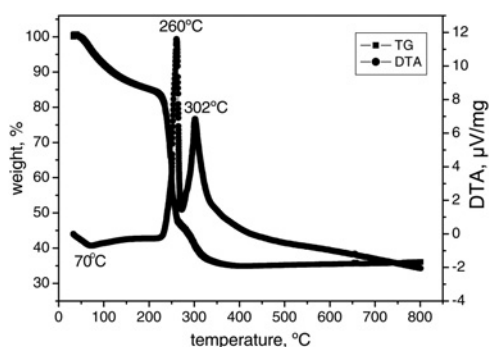


Figure 2 TG–DSC curves of the gel precursor

centred at 3450 cm^{-1} is because of the hydroxyl groups of chemisorbed and/or physisorbed H_2O molecules [15]. The broad absorption from 2450 to 3100 cm^{-1} is ascribed to O–H bond stretching of the –COOH group. The broad and strong absorption from 1630 to 1730 cm^{-1} is the characteristic peaks of C=O bond stretching of three types of –COOH groups. The broad absorption peak from 1040 to 1500 cm^{-1} is caused by the coupling of O–H in-plane bending vibration and C–O stretching in dimmers of citric acids [16].

In the FTIR spectrum of the gel precursor shown in Fig. 1b, the broad absorption at 3400 cm^{-1} is from O–H stretching vibrations of ethanol molecules and water molecules adsorbed to the gel. The broad absorptions at 3000 and $1260\text{--}1428\text{ cm}^{-1}$ are from C–H stretching and C–H bending vibrations of ethanol molecules, respectively. The absorption peaks at 620 and 680 cm^{-1} are attributed to the stretching vibrations of Li–O and Mn(II)–O bonds [17], respectively. Moreover, the strong absorption peaks of C–O and C=O bonds stretching ($1020\text{--}1090\text{ cm}^{-1}$ and $1500\text{--}1700\text{ cm}^{-1}$) in the gel precursor have a blue shift in comparison with those of pure citric acid, because of –OM (M, metal) groups in place of –OH groups. The results from the FTIR spectra indicate that the citric acid plays the role of chelating agent. Therefore the main compositions of the gel precursor are Li–CA (CA, citric acid), Mn–CA and/or Li–CA–Mn complex compounds.

Fig. 2 shows TG–DTA curves of the gel precursor. The weight loss of 26% ranging from 40 to 220°C is from the evaporation of residual ethanol molecules and a small quantity of water molecules adsorbed to the gel from air. The small endothermic peak at 70°C is caused by the evaporation of ethanol. There is a huge weight loss of 50% at $220\text{--}350^\circ\text{C}$, resulting from thermal decomposition of organic parts of the gel precursor. During the thermal decomposition, there was a large quantity of heat releasing. The released heat firstly promoted the formation of Mn_2O_3 [14], accompanying with the exothermic peak at 260°C . The pyrolysis of the remaining organic parts released

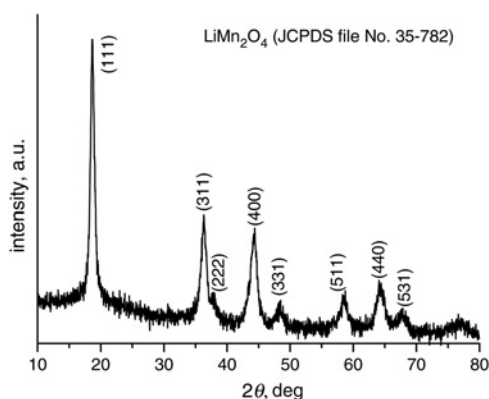


Figure 3 XRD pattern of the as-prepared sample

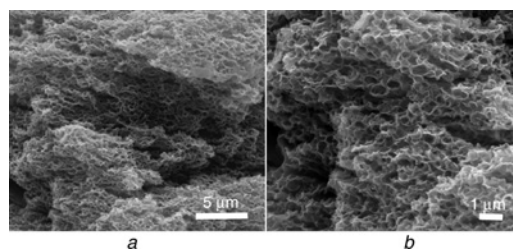


Figure 4 SEM images of the as-prepared sample
a Under low magnification
b Under high magnification

heat to promote the formation of the LiMn_2O_4 phase corresponding to the exothermic peak centred at 302°C . The weight is nearly constant when the temperature is above 370°C .

3.2. Phase structure of the as-prepared LiMn_2O_4 : The XRD pattern of the product is shown in Fig. 3. The diffraction pattern is in good agreement with LiMn_2O_4 JCPDS Card No. 35-0782. No other crystal phase or obvious impurity peaks are detected. All the diffraction peaks originate from the cubic spinel structure with space group $\text{Fd}\bar{3}m$, wherein the lithium ions occupy 8a sites, manganese ions 16d sites and oxygen ions 32e sites. The broadening diffraction peaks suggest that the size of as-fabricated LiMn_2O_4 should be very small. According to the Scherrer equation [18], the size of LiMn_2O_4 was estimated to be 8 nm by choosing three strong peaks of (111), (311) and (400).

3.3. Morphology and microstructure of the as-prepared LiMn_2O_4 : Fig. 4a shows a low-magnification SEM image of the as-prepared spinel LiMn_2O_4 , which displays a three-dimensional honeycomb-like porous structure from a general view. These holes are in the shape of quasi-hemispheres. The distribution of these holes is not in order but homogeneous. A high-magnification SEM image in Fig. 4b further shows a full-developed porous structure. The diameter of pores is 700 nm or so and the walls of pores are very thin. The details of porous nanostructures are further analysed by TEM and HRTEM techniques.

Fig. 5a presents a TEM image of the as-fabricated porous nanostructures through a high-strength ultrasonic in absolute ethyl alcohol. There are brightness and darkness sections in the image, indicating the resulting product is of a porous structure as well. The dark region is the bulk of porous structures and the bright region is the pores. In addition, Fig. 5a shows that the bulk section of honeycomb-like porous structures is composed of nanocrystallines. The high-magnification TEM image shown in Fig. 5b displays the size of nanocrystalline is of about 10 nm. The observation is larger than the estimation size by the Scherrer equation, for the peak's broadening caused by equipment has not been deducted from the full-width at half-maximum intensity of the diffraction peak in the act of calculation.

Fig. 5b also shows nanocrystallines fused together forming a slit-pored structure. The results from the analysis of the SEM and TEM images demonstrate that the resulting material is a dual-porous nanostructure. An HRTEM image in Fig. 5c shows differently oriented nanocrystallines. There are two kinds of interplanar spacings. One is 0.2841 nm and the other is 0.4812 nm, corresponding to the crystal planes of (220) and (111), respectively. The regions denoted by circles show fused sections among nanocrystallines.

3.4. Specific surface area and pore sizes of the as-prepared sample: The full nitrogen sorption isotherm of the hierarchical LiMn_2O_4 porous nanostructures was measured to gain information about the specific surface area and the pore size. As shown in Fig. 6, the

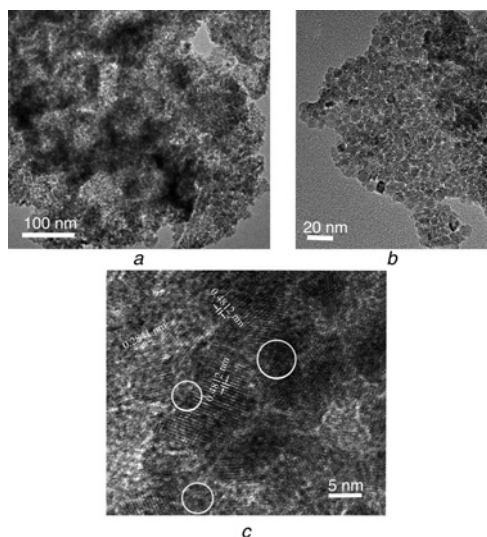


Figure 5 TEM images and HRTEM image of the as-prepared spinel LiMn_2O_4

a Under low magnification

b Under high magnification

These show that the honeycomb-like porous nanostructure is composed of ultrafine nanocrystallines of about 10 nm

c HRTEM image of the as-prepared spinel LiMn_2O_4 , showing the partial fusion among ultrafine nanocrystallines marked with circles

nitrogen sorption isotherm can be identified as type V according to the IUPAC category [19], suggesting that the as-fabricated spinel LiMn_2O_4 possesses a few micropores and a large quantity of mesopores. The inset in Fig. 6 shows the corresponding pore-size distribution from the Barrett-Joyner-Halenda (BJH) desorption. The sizes of pores mainly fall into 3–10 nm, and the cumulative pore volume is $0.205 \text{ cm}^3/\text{g}$. The specific surface area is calculated to be $116 \text{ m}^2/\text{g}$ by the BET equation, which is larger than reported spinel LiMn_2O_4 nanoparticles, to the best of our knowledge. The high surface area and dual-porous nanostructure of the as-fabricated spinel LiMn_2O_4 can provide an efficient diffusion and transportation of Li ion in the lithium battery, which would improve the electrochemical performance of the LiMn_2O_4 cathode.

3.5. Effects on the formation of LiMn_2O_4 porous nanostructures: Based on the analysis of the FTIR spectrum of the gel precursor, the main compositions of the gel precursor are complex compounds of $\text{Li}^+/\text{Mn}^{2+}$ combined with CA. When the gel precursor was annealed in air, some organic parts of complex compounds would begin to pyrolyse into volatile gases of H_2O

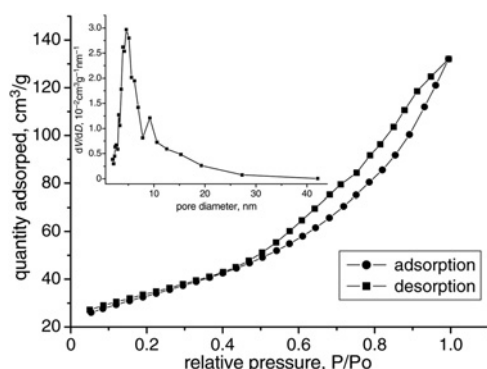


Figure 6 Typical nitrogen gas adsorption-desorption isotherm of the as-prepared sample, displaying the feature of mesoporous materials
Inset: Corresponding to differential pore-size distribution

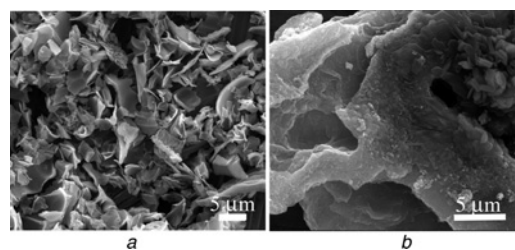


Figure 7 SEM images of the products prepared using different amount of citric acid, keeping other fabricated parameters unvaried

a 0.5 g

b 2.0 g

and CO_2 and produce original vacancies. According to the Kirkendall effect, the original vacancies for balancing the released atoms could condense into voids [20]. As the pyrolysis proceeded, the amount and diffusion rate of volatile gases increased, producing new voids and coalescing of part of old voids. When some old voids became congregation centres, macropores began to form driven by surface diffusion [21]. As a result, the formation of porous nanostructures should be attributed to the Kirkendall effect and surface diffusion. To confirm the effects from the diffusion rate of H_2O and CO_2 gases on the formation of pores, comparative experiments were carried out.

Fig. 7 shows SEM images of spinel LiMn_2O_4 obtained using different amounts of citric acid, keeping other fabrication parameters unvaried. Using citric acid of 0.5 g, the product is rigid fragments without macropores (shown in Fig. 7a). When the amount of combusting agent decreased, the amount and diffusion rate of released volatile gas would reduce; it suppressed formation of new voids and the coalescence of old ones. Simultaneously, the reaction heat also reduced and thermal expansion was weakened, which hindered the formation of macropores. When the amount of citric acid increased to 2.0 g, the amount and diffusion rate of H_2O and CO_2 gas increased and thermal expansion was strengthened. As a result, coalescing of old voids was speeded up, leading to producing large air holes, as shown in Fig. 7b.

In addition to the amount of combusting agent, the heating rate of gels also has an effect on the releasing rate of volatile gases. Fig. 8 shows SEM images of spinel LiMn_2O_4 obtained at different heating rates. The LiMn_2O_4 prepared at a heating rate of $2^\circ\text{C}/\text{min}$ is fluffy and fragile and its morphology looks like different-size bowls packed together. The lowering of heating rate causes the slowing of the released rate of volatile gases produced by pyrolysis of organic parts of gels. On the one hand, it prevents original voids from coalescing; on the other hand, it prolongs the releasing time of volatile gases, which would promote mass transfer along the inward surface of pores driven by surface diffusion and lead to the growth of bowl-like shapes around the holes (shown in Fig. 8b). However, when the heating rate increases to $15^\circ\text{C}/\text{min}$, the obtained spinel becomes small particles (shown in Fig. 8b). The fast heating rate

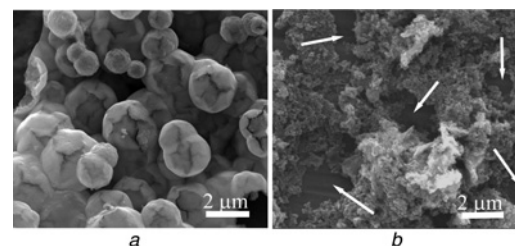


Figure 8 SEM images of the products prepared at different heating rates, keeping other fabricated parameters unvaried

a $2^\circ\text{C}/\text{min}$

b $15^\circ\text{C}/\text{min}$

speeds up releasing of reaction heat and volatile gases; the fast giving off heat and gases quickens the coalescence of voids and the formation of macropores so that all voids and macropores break up to particles under thermal expansion and inside pressure.

Depending on the discussions described above, the amount of combusting agent and heating rate must be appropriate for precursor-pyrolysing fabrication of LiMn_2O_4 porous nanostructures at lower temperature.

4. Conclusions: Hierarchical spinel LiMn_2O_4 porous nanostructures were obtained by a precursor-pyrolysing method. The citric acid plays the roles of chelating and combusting agent. The hierarchical porous nanostructures present hemispherical macropores and slit mesopores. Their building units are nanocrystallines of about 10 nm. The BET-specific surface area of the spinel LiMn_2O_4 hierarchical porous nanostructure is $116 \text{ m}^2/\text{g}$. The heating rate and the amount of complexing agent have important effects on the formation of dual-porous LiMn_2O_4 nanostructures. These dual-porous nanostructures and the large specific surface area are promising to enhance the electrochemical behaviours of LiMn_2O_4 cathode in a lithium battery.

5. Acknowledgments: The work was financially supported by the Qianjiang Talent Project of Science Technology Department in Zhejiang Province (grant no. 2012R10077) and the Zhejiang Province Natural Science Foundation (grant numbers Y4110641 and Y4100471).

6 References

- [1] Park H.S., Hwang S.J., Choy J.H.: 'Relationship between chemical bonding character and electrochemical performance in nickel-substituted lithium manganese oxides', *J. Phys. Chem. B*, 2001, **105**, pp. 4860–4866
- [2] Zhao C.H., Kang W.P., Wang X.X., Zhao S.Q., Shen Q.: 'Sacrificial templating synthesis of rod-like $\text{LiNi}_x\text{Mn}_{2-x}\text{O}_4$ spinels and their improved cycling performance', *Micro Nano Lett.*, 2012, **7**, pp. 558–560
- [3] Jayalakshmi M., Rao M.M., Scholz F.: 'Electrochemical behavior of solid lithium manganate (LiMn_2O_4) in aqueous neutral electrolyte solutions', *Langmuir*, 2003, **19**, pp. 8403–8408
- [4] Lee Y.S., Sun Y.K., Nahm K.S.: 'Synthesis of spinel LiMn_2O_4 cathode material prepared by an adipic acid-assisted sol-gel method for lithium secondary batteries', *Solid State Ion.*, 1998, **109**, pp. 285–294
- [5] Hwang B.J., Wang C.Y., Cheng M.Y., Santhanam R.: 'Structure, morphology, and electrochemical investigation of LiMn_2O_4 thin film cathodes deposited by Radio frequency sputtering for lithium microbatteries', *J. Phys. Chem. C*, 2009, **113**, pp. 11373–11380
- [6] Shaju K.M., Bruce P.G.: 'A stoichiometric nano- LiMn_2O_4 spinel electrode exhibiting high power and stable cycling', *Chem. Mater.*, 2008, **20**, pp. 5557–5562
- [7] Kamarulzaman N., Yusoff R., Kamarudin N., ET AL.: 'Investigation of cell parameters, microstructures and electrochemical behaviour of LiMn_2O_4 normal and nano powders', *J. Power Sources*, 2009, **188**, pp. 274–280
- [8] Kiani M.A., Mousavi M.F., Rahmanifar M.S.: 'Synthesis of nano- and micro-particles of LiMn_2O_4 : electrochemical investigation and assessment as a cathode in Li battery', *Int. J. Electrochem. Sci.*, 2011, **16**, pp. 2581–2595
- [9] Chen Y.C., Xie K., Pan Y., Zheng C.M., Wang H.L.: 'High power nano- LiMn_2O_4 cathode materials with high-rate pulse discharge capability for lithium-ion batteries', *Chin. Phys. B*, 2011, **20**, p. 028201
- [10] Liu H., Wu Y.P., Rahm E.: 'Cathode materials for lithium ion batteries prepared by sol-gel methods', *Solid-State Electron.*, 2004, **8**, pp. 450–466
- [11] Wu S.H., Chen H.L.: 'The effects of heat-treatment temperature on the retention capacities of spinels prepared by the Pechini process', *J. Power Sources*, 2003, **119**, pp. 134–138
- [12] Ting-Kuo F.G., Cho Y.D., Kumar T.P.: 'Nanocrystalline LiMn_2O_4 derived by HMTA-assisted solution combustion synthesis as a lithium-intercalating cathode material', *Mater. Chem. Phys.*, 2006, **99**, pp. 451–458
- [13] Liu Z.Q., Wang W.I., Wu M.C.: 'Hydrothermal synthesis of nanostructured spinel lithium manganese oxide', *J. Solid State Chem.*, 2004, **177**, pp. 1585–1591
- [14] Tong Y.H., Shao M.W., Ni Y.B., Qian G.X., Ye Y., Zhang P.: 'Low temperature route to nanocrystalline LiMn_2O_4 spinel', *Mater. Lett.*, 2006, **60**, pp. 2578–2581
- [15] Vivekanandhan S., Venkateswarlu M., Satyanarayana N.: 'Novel urea assisted polymeric citrate route for the synthesis of nanocrystalline spinel LiMn_2O_4 powders', *J. Alloy Compd.*, 2007, **441**, pp. 284–290
- [16] Socrates G.: 'Infrared and Raman characteristic group frequencies' (John Wiley and Sons, New York, 2001)
- [17] Lei G.T., Li Z.H., Su G.Y.: 'The preparation of spinel LiMn_2O_4 ', *Battery Bimonth.*, 2003, **33**, pp. 164–166
- [18] Patterson A.L.: 'The Scherrer formula for x-ray particle size determination', *Phys. Rev.*, 1939, **56**, pp. 978–982
- [19] Ryu Z.Y., Zheng J.T., Wang M.Z.: 'Characterization of pore size distributions on carbonaceous adsorbents by DFT', *Carbon*, 1999, **37**, pp. 1257–1264
- [20] Smigelskas A.C., Kirkendall E.O.: 'Zinc diffusion in alpha brass', *Trans. Am. Inst. Mining Metall. Petroleum Eng.*, 1947, **171**, pp. 130–142
- [21] Fan H.J., Knez M., Scholz R., ET AL.: 'Influence of surface diffusion on the formation of hollow nanostructures induced by the Kirkendall effect: The basic concept', *Nano Lett.*, 2007, **7**, pp. 993–997